LANGMUIR

pubs.acs.org/Langmuir Article

Effect of Extra Gas Amount on Liquid Outflow from Hydrophobic Nanochannels: Enhanced Liquid—Gas Interaction and Bubble Nucleation

Mingzhe Li, Lijiang Xu, and Weiyi Lu*



Cite This: Langmuir 2020, 36, 4682-4688



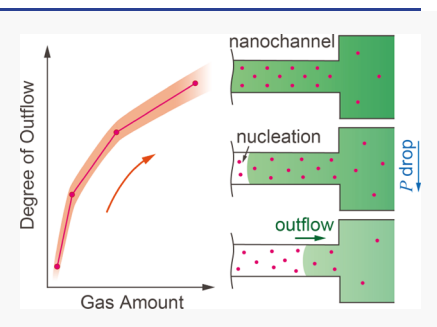
ACCESS

III Metrics & More



Supporting Information

ABSTRACT: Understanding liquid motion in nanoenvironment is of fundamental importance in nanofluidics-based systems. While the liquid outflow from hydrophobic nanochannels can significantly affect system performance, its underlying mechanism remains unclear so far. Here, we present an experimental study of the gas-phase effect on liquid outflow behavior from hydrophobic nanochannels in a liquid nanofoam (LN) system. Four LN samples, consisting of same liquid—solid composition but different amounts of the gas phase, are characterized by cyclic quasi-static compression tests. A remarkable difference in the LN system reusability has been observed, indicating that the liquid outflow behavior is highly sensitive to the amount of the gas phase. As the gas amount increases, the degree of liquid outflow from hydrophobic nanochannels is considerably promoted. This promotive effect is because of the suppression of gas outflow



and acceleration of bubble nucleation in the nanochannels. These fundamental findings open a new perspective on liquid outflow behavior and can facilitate the design of reusable nanofluidics-based energy absorbers.

INTRODUCTION

Liquid flow in nanochannels is of great importance for a variety of applications, including water filtration, 1,2 drug delivery, 3,4 heterogeneous catalysis, 5,6 chemical and bio-sensing, 7,8 and many others. Especially, forced liquid flow in hydrophobic nanochannels is employed as a novel mechanism for energy storage and mitigation in a liquid nanofoam (LN) system. ^{9–11} In an LN system composed of a hydrophobic nanoporous media and a nonwetting liquid, the liquid molecules are forced into the nanochannels when the applied external load is sufficient to overcome the capillary force. As the external load is removed, the intruded liquid can be fully or partially expelled from the hydrophobic nanochannels. 12,13 Because of its highly hysteretic mechanical response, tremendous amount of energy is mitigated by the LN system. With the liquid outflow, the LN system recovers its energy mitigation capacity and is capable of mitigating repetitive impacts. The system recoverability of LN is determined by the degree of liquid outflow from the hydrophobic nanochannels during the load releasing process. Therefore, understanding the underlying mechanism of this confined liquid outflow behavior is essential to develop advanced energy absorption system for repetitive impacts in sports, battlefield, and transportation. Moreover, the elucidation and manipulation of the nanoscale liquid outflow will provide important insights and immediate guidance for designing other systems consisting of liquid and nanoporous media such as thermal actuators 14,15 and ionic-liquid-based supercapacitors.16

The liquid outflow from hydrophobic nanochannels has been studied by many researchers, and it has been found that the liquid outflow behavior in nanoenvironment is related to the excessive liquid-solid interfacial tension, ¹⁷⁻¹⁹ nanoporous structure, 20 and liquid—gas interaction. 21 For example, the addition of potassium chloride increases the excessive liquidsolid interfacial tension of the LN system and promotes the degree of liquid outflow. 17 The effect of liquid-solid interaction on liquid outflow from hydrophobic nanochannels in the absence of gas phase has been well explained by nanoscale vapor bubble nucleation theory. 22-24 During the unloading process, the hydrophobic confinement facilitates the nucleation and growth of a vapor cavity, which is accompanied by the continuous outflow of confined liquid phase. In addition to the liquid-solid interaction in the nanoenvironment, it has also been demonstrated that the liquid-gas interaction in the nanoenvironment significantly affects the nanoscale liquid outflow. Through MD simulation, Qiao et al.21 have quantitatively validated that even a single gas molecule makes the confined liquid unstable. The gas molecules in nanochannels tend to form clusters and trigger liquid outflow. In our previous works, 12,25 it has been demonstrated that

Received: February 18, 2020 Revised: April 17, 2020 Published: April 17, 2020





reduced gas solubility in the bulk liquid phase combining with enhanced gas oversolubility in the confined liquid phase preserves more gas molecules in the nanochannels and endows the LN system with higher degree of liquid outflow. Sun et al. 26 also reported that liquid outflow has been improved by hindering the time-dependent mass transportation in the nanochannels. However, experimental studies on the gas-phase effect are still scarce. There is lack of a comprehensive understanding of the mechanism underpinning liquid outflow and the fundamentals of liquid—gas interaction in the nanoenvironment. An experimental approach to individually investigate the gas phase effect on liquid outflow is in high demand.

In this study, we have thoroughly studied the gas-phase effect on the liquid outflow by introducing different amounts of gas into LN systems with a constant excessive liquid—solid interfacial tension. The degree of liquid outflow in these LN systems is characterized by cyclic quasi-static compression tests. The results show that the degree of liquid outflow is promoted as the amount of gas increases. Further theoretical analysis reveals that the fast gas saturation of the bulk liquid and the enhanced bubble nucleation in the hydrophobic nanochannels suppress gas outflow but promote liquid outflow.

■ EXPERIMENTAL SECTION

Materials. The nanoporous material used in current study was hydrophilic nanoporous silica (SP-120-20, DAISO Fine Chem USA, INC.). The as-received material was in powder form, with an average pore size of 12 nm and particle size around 20 μ m (Figure S1 in Supporting Information). The specific pore volume of the nanoporous silica was 700 mm³/g. To make its surface hydrophobic, a thin layer of chloro(dimethyl)octylsilane was anchored onto the nanopore surface, as previously reported. ^{13,27} Briefly, 1 g of silica gel was mixed with 40 mL of anhydrous toluene. Chloro(dimethyl)octylsilane (10 mL) and pyridine (1 mL) were then injected into the mixture. The mixture was gently stirred at 95 °C for 18 h, after which the surface-treated silica gel was filtered, washed with ethanol, and dried for at least 24 h before use. The liquid phase of the LN was deionized (DI) water.

Sample Preparation. The LN sample was prepared by sealing 0.2 g of surface-treated silica gel and 1.5 mL of DI water in a stainless steel testing cell with two O-ring equipped pistons, as shown in Figure 1a. The cross-sectional area of the pistons, A, was 286 mm². Four types of LN samples were prepared with the same amount of silica gel and DI water but different amounts of gas phase, that is, air. The LN sample, denoted as LN-V (Figure 1b), was prepared by placing the mixture in vacuum (<3 kPa) for several hours to minimize the amount of air in the nanochannels and the bulk liquid phase. The LN sample prepared at ambient condition without degassing was denoted as LN-N, which contained small amount of air trapped in between hydrophobic silica gel particles (Figure 1c). Extra gas was introduced into the LN sample by sealing an additional air column in the testing cell, forming LN sample LN-EL and LN-EM (Figure 1d). The detailed LN sample information is summarized in Table 1. The gas volume in the nanochannels was calculated as $V_i = m \cdot V_{sp}$, where m and $V_{\rm sp}$ were the mass and specific pore volume of the silica gel, respectively. The volume of extra gas in the LN was determined by $V_{
m o}$ = $A \cdot l - (V_{DI} + m/\rho + V_i)$, where l is the total length of the sealed LN sample, V_{DI} is the volume of DI water, and ρ is the density of silicon dioxide. The gas-to-liquid volume ratio of the prepared LN samples at ambient condition was calculated as $\phi = (V_{\rm i} + V_{\rm o})/V_{\rm DI}$.

Quasi-Static Compression Test. The LN sample sealed in the testing cell was compressed by a universal tester (Floor model 5982, Instron, Inc.) at a speed of 2 mm/min. For each type of LN, three samples were tested. The applied force, *F*, increased gradually to 10 kN, leading to an equivalent pressure of 35 MPa in the testing cell. As the peak force was reached, the Instron crosshead was moved back at the same speed. To study the liquid outflow behavior of the LN, the

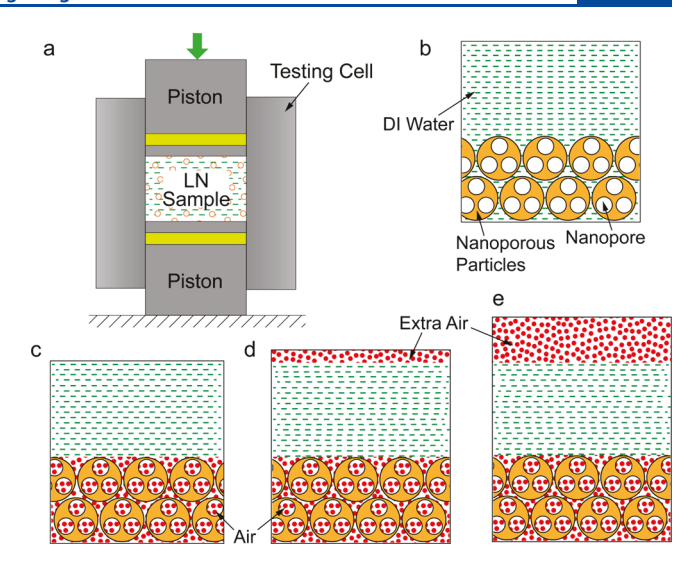


Figure 1. Schematic of the experimental setup and LN samples containing various amounts of air: (a) quasi-static compression test of LN sample sealed in a testing cell, (b) degassed LN sample, LN-V, (c) LN sample without degassing, LN-N, (d) LN sample with lower amount of extra gas, LN-EL, and (e) LN sample with higher amount of extra gas, LN-EM.

Table 1. LN Sample Information

| sample | m (g) | $V_{\mathrm{DI}}\ (\mathrm{mL})$ | $V_{\rm i}~({ m mL})$ | $V_{\rm o}~({\rm mL})$ | $P_{\rm d}$ (MPa) | φ (%) |
|--------|-------|----------------------------------|-----------------------|------------------------|-------------------|-------|
| LN-V | 0.2 | 1.5 | 0 | 0 | 0 | 0 |
| LN-N | 0.2 | 1.5 | 0.14 | 0.08 | 0.3 | 15 |
| LN-EL | 0.2 | 1.5 | 0.14 | 0.75 | 2.9 | 60 |
| LN-EM | 0.2 | 1.5 | 0.14 | 1.95 | 7.7 | 140 |
| | | | | | | |

compression test was repeated at least three times for each LN sample. The hydrostatic pressure in the testing cell was calculated as P = F/A. The specific volume change of the LN sample was calculated as $\Delta V = A \cdot \delta/m$, where δ is the measured piston displacement and m is the mass of the silica gel (Table 1).

■ RESULTS AND DISCUSSION

Figure 2a shows typical consecutive loading-unloading cycles of an LN sample. Only the first and second loading-unloading cycles are shown here because all subsequent cycles are nearly identical to the second one. At ambient condition, the water molecules stay outside of the nanochannels because of the surface hydrophobicity. As the external force is applied, initially, the mechanical response of LN samples is nearly elastic and the system bulk moduli are contributed by both liquid and solid compositions. When the pressure reaches approximately 13 MPa, the slope of the loading curve shows considerable reduction, and an infiltration plateau with the smallest slope of the loading curve is formed. This corresponds to the water molecules being forced into the nanochannels, referred to as the liquid infiltration process. The pressure at which liquid infiltration occurs is defined as the liquid infiltration pressure, $P_{\rm in}$, which is governed by the classic Laplace-Young equation, $P_{\rm in} = 2\Delta \gamma/r$, where $\Delta \gamma$ is the excessive solid-liquid interfacial tension and r is the nanochannel radius. As all the nanochannels are filled with water molecules, the liquid infiltration plateau ends as indicated by the next turning point at 22 MPa. The effective nanochannel volume of the LN, which is determined by the width of the infiltration plateau ω_1 , is around 730 mm³/g. Thereafter, the LN system becomes elastic again. Upon

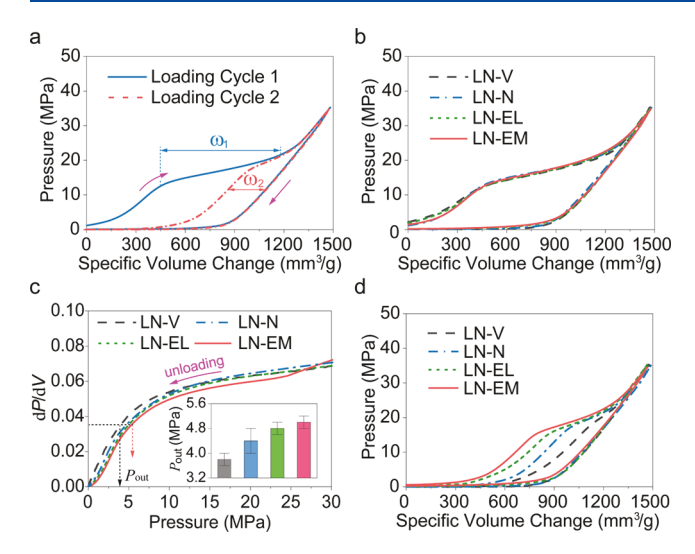


Figure 2. Quasi-static compression testing results of different LN samples: (a) typical consecutive loading—unloading cycles of an LN sample, (b) typical first loading—unloading cycles of different LN samples, (c) reduced slope of the unloading curves in the first cycles of different LN samples, and (d) typical second loading—unloading cycles of different LN samples.

unloading, the pressure drops quickly in a linear manner at the beginning. As the pressure further reduces, the slope of the unloading curve starts to decrease. The reduced slope of the unloading curve as well as the associated specific volume change indicate the combined liquid and gas outflow from the hydrophobic nanochannels.

When the external pressure is removed, both confined gas and liquid molecules start to flow out from the nanochannels. It is difficult to quantify the volume of liquid outflow by analyzing the unloading curve. Instead, the width of the liquid infiltration plateau in the second loading-unloading cycle is a direct measure. In the second cycle, the LN system shows a similar hysteric loading-unloading response. However, compared with the first cycle, $P_{\rm in}$ is increased, while the width of the infiltration plateau, ω_2 , is much smaller. The reduced infiltration plateau width suggests that only a partial nanochannel volume is available in the second cycle, which is due to the partial liquid outflow from the nanochannels in the first cycle. The volume of the liquid outflow is equivalent to the volume of gas retained in the hydrophobic nanochannels. Therefore, the degree of liquid outflow from nanochannels or the degree of gas retention in the nanochannels, η_{out} , is defined as

$$\eta_{\text{out}} = \omega_2/\omega_1 \tag{1}$$

Figure 2b shows the typical first loading—unloading cycles of four LN samples. The curves are shifted along the α -axis for better comparison. During the loading process, the mechanical response of four LN samples is nearly the same; that is, neither the effective pore volume ω_1 nor the liquid infiltration pressure $P_{\rm in}$ of the LN is affected by the considerably increased amount of gas phase. Because all the LN samples possess the same $P_{\rm in}$, according to the classic Laplace—Young equation, the excessive surface tension at the solid—liquid—gas interface is a constant. The additional gas content has negligible effect on the interfacial tension. As the excessive solid—liquid—gas interfacial tension significantly affects the liquid outflow behavior, 18,19 maintaining it as a constant is crucial for the investigation of

the gas phase effect. The constant solid—liquid—gas interface is attributed to the hydrophobic nanopore surface. As water molecules meet the hydrophobic surface, a thermodynamically driven depletion layer is formed. ²⁸ In the depletion layer, the low-density hydrogen bonds are highly orientated, preclude the existence of gas molecules, and dominate the solid—liquid—gas interface. Thus, the dissolved gas molecules exhibit negligible effects on the interfacial tension. During unloading, the fast linear reduction in system pressure ends at a higher pressure when the LN sample contains larger gas volume. The above-described identical loading process and difference in unloading process indicate that the additional gas volume in LN systems has prominent effect on the combined gas and liquid outflow from the hydrophobic nanochannels.

When the linear unloading ends, the system volume expands more with unit pressure reduction. This indicates confined gas and liquid molecules flow out from the nanochannels and the corresponding critical pressure is defined as the outflow pressure, $P_{\rm out}$. To further quantify $P_{\rm out}$ the slope of the unloading curves $({\rm d}P/{\rm d}V)$ is plotted versus the system pressure in Figure 2c. The increased $V_{\rm o}$ reduces the effective bulk modulus of the resulted LN samples, which is validated by the reduced slope from 30 to 15 MPa. $P_{\rm out}$ is quantified when the slope $({\rm d}P/{\rm d}V)$ is reduced to 0.35 and increases from 3.8 MPa (LN-V) to 5.1 MPa (LN-EM) with increasing ϕ (inset in Figure 2c and Table 2). Concurrently, ω_2 monotonically

Table 2. Measured Effective Pore Volume and Calculated Degree of Liquid Outflow of Different LN Samples

| sample | $\omega_1 (\text{mm}^3/\text{g})$ | $\omega_2 (\mathrm{mm}^3/\mathrm{g})$ | η _{out} (%) | P _{out} (MPa) |
|--------|------------------------------------|--|----------------------|------------------------|
| LN-V | 730 ± 9 | 119 ± 8 | 16 ± 1 | 3.8 ± 0.2 |
| LN-N | 732 ± 7 | 232 ± 11 | 32 ± 1 | 4.4 ± 0.4 |
| LN-EL | 736 ± 9 | 330 ± 13 | 45 ± 2 | 4.8 ± 0.2 |
| LN-EM | 727 ± 7 | 407 ± 17 | 56 ± 2 | 5.0 ± 0.2 |

increases with increasing ϕ (Figure 2d and Table 2). Because all the LN samples have similar ω_1 , $\eta_{\rm out}$ increases from 16 to 56% with the promoted $P_{\rm out}$ (Figure 3a and Table 2), as ϕ

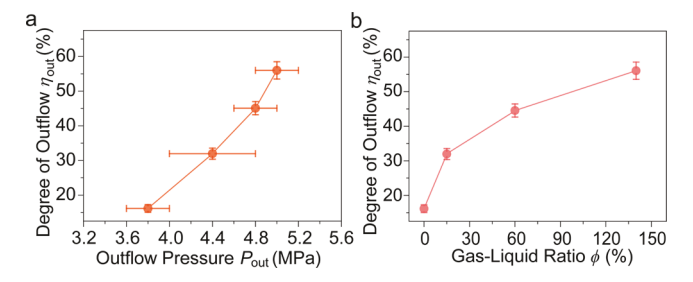


Figure 3. Degree of liquid outflow as a function of (a) $P_{\rm out}$ the outflow pressure, and (b) ϕ , the gas—liquid ratio.

increases from 0 to 140% (Figure 3b). The degree of liquid outflow is significantly enhanced by the only system variable, that is, the extra gas in the LN systems.

At the molecular level, as all the LN samples have identical excessive solid–liquid interfacial tension, the variation in $\eta_{\rm out}$ is attributed to the enhanced liquid–gas interaction in the nanochannels in the unloading process. During the loading process, the system pressure gradually increases and gas molecules are dissolved into the bulk and confined liquid phases in a stepwise manner (Figure 4a–c). First, the gas

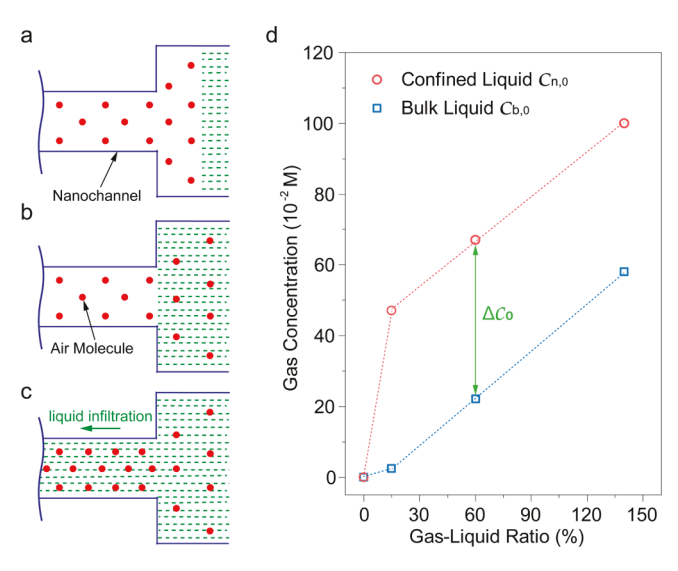


Figure 4. (a-c) Stepwise gas molecule dissolution into the bulk and confined liquid phases and (d) gas concentration in the bulk and confined liquid at peak pressure.

outside nanochannels are dissolved into the bulk liquid (Figure 4b). According to Henry's law, the bulk gas solubility is proportional to the system pressure²⁹

$$C_{g} = P_{g}/k_{H,T} \tag{2}$$

where $C_{\rm g}$ is the gas solubility in bulk liquid, $P_{\rm g}$ is the partial pressure of gas, and $k_{H,T}$ is the Henry's coefficient at temperature T. At 1 atm, the air solubility is 7.6×10^{-4} M. The pressure at which all the extra air molecules outside nanochannels are dissolved into the bulk liquid phase, denoted as P_{dy} is calculated and summarized in Table 1. P_{d} is much smaller than the infiltration pressure $P_{\rm in}$. Therefore, all the air molecules outside nanochannels are fully dissolved into the bulk liquid phase before liquid infiltration occurs. During liquid infiltration process, the bulk liquid phase (both water and dissolved air molecules) starts to enter the nanochannels and dissolves the confined air molecules. As demonstrated by many researchers, ^{12,30-33} the gas solubility in the confined liquid phase in the nanochannels, also known as gas oversolubility, is more than 10 times higher than the solubility in the bulk liquid phase. Therefore, all air molecules inside the nanochannels are fully dissolved by the intruded liquid phase (Figure 4c). The calculated gas concentration in the bulk liquid $c_{\rm b,0}$ as well as in the nanochannels $c_{n,0}$ are summarized in Table 3 and plotted in

Table 3. Gas Concentration in the Bulk Liquid, $c_{b,0}$, and Gas Concentration in the Nanochannels, $c_{n,0}$, at Peak Pressure

| sample | $c_{b,0}$ (M) | $c_{\rm n,0}~({ m M})$ | Δc_0 (M) |
|--------|----------------------|------------------------|----------------------|
| LN-V | 0 | 0 | 0 |
| LN-N | 2.4×10^{-3} | 4.7×10^{-2} | 4.4×10^{-2} |
| LN-EL | 2.2×10^{-2} | 6.7×10^{-2} | 4.4×10^{-2} |
| LN-EM | 5.8×10^{-2} | 1.0×10^{-1} | 4.4×10^{-2} |

Figure 4d. The values of $c_{\rm b,0}$ and $c_{\rm n,0}$ increase with ϕ , while the concentration difference $\Delta c_0 = (c_{\rm b,0} - c_{\rm n,0})$ is a constant. As shown in Table 3, for LN-EM sample with the highest amount of gas, $c_{\rm n,0}$ is only ~2 times of $c_{\rm b,0}$, indicating that the confined liquid phase in the nanochannels is far from saturation.

As the unloading process begins, the initial linear response (Figure 2b) is due to the linear volume expansion of the bulk liquid phase resulted from the reduced system pressure. As the total volume change of the LN systems is small and the sudden pressure drop (\sim 20 MPa reduction in 5 s), the liquid outflow from the nanochannels to the bulk liquid phase is limited and negligible.

When the linear unloading ends $(dP/dV \approx 0.06)$ in Figure 2c), instead of the linear volume expansion, the combined liquid and gas outflow from the nanochannels to the bulk liquid phase dominates the system volume recovery. Particularly, the gas outflow includes gas diffusion and advection from the nanochannels to the bulk liquid phase. As stated in Fick's law,³⁴ the gas diffusion flux is directly proportional to the concentration gradient. Because Δc_0 is a constant for all LN samples except LN-V, the initial gas molecule diffusion rates are exactly the same. In addition, the gas diffusion is a slow process, given the unloading process is completely in less than a minute, the amount of gas diffusing from the nanochannels to the bulk liquid phase can be ignored.

The gas advection is defined as the dissolved gas molecules flow out from the nanochannels to the bulk liquid phase with the liquid, driven by the increased intermolecular spacing in the nanochannels. The gas advection flux is proportional to the mass-transfer velocity and the gas concentration at the interface between nanochannels and the bulk liquid phase. Because the system volume recovery is controlled at a constant rate (2 mm/min), the initial mass-transfer velocities of all LN samples are the same. The advection-induced gas concentration reduction is

$$\Delta c_{n,a}(t) = \int_0^t k_a(\tau) \cdot c_n(\tau) d\tau$$
(3)

where $k_{\rm a}$ is a time-dependent parameter and $c_{\rm n}$ is the gas concentration in liquid confined in the nanochannels at time τ . The gas outflow process leads to gas concentration decrease in the confined liquid and increase in the bulk liquid (Figure 5a,b).

Given the large and quick pressure drop in the linear unloading process, the bulk gas solubility is reduced accordingly based on Henry's law. Therefore, the gas molecules escaped from the nanochannels quickly saturate the bulk liquid phase. As the bulk liquid phase is not capable of accommodating more gas molecules, the gas outflow from the nanochannels is blocked (Figure 5b). The critical pressure, at which the gas saturation occurs, is defined as the blocking threshold pressure of gas outflow, $P_{\rm t}$. Given $c_{\rm n,0} \geq c_{\rm b,0}$, the liquid flowing out from the nanochannels has higher gas concentration than that of the liquid intrudes into the nanopores during the loading process. Therefore, with the additional gas outflow, the bulk liquid phase is saturated at higher pressure $(P_{\rm t} > P_{\rm d})$ for a given LN system. The total time needed to saturate the bulk liquid phase is defined as the threshold time of gas outflow, t_0 .

When the bulk liquid is saturated during the unloading process, the bulk gas concentration is

$$c_{\rm b}(t_0) = c_{\rm b,0} + \frac{V_{\rm i}}{V_{\rm DI} - V_{\rm i}} \Delta c_{\rm n,a} = P_{\rm t}/k_{\rm H,T}$$
 (4)

Accordingly, the bulk gas concentration increase contour in LN specimens is qualitatively sketched versus the system pressure in Figure 5d. For LN samples with extra gas, both $c_{b,0}$

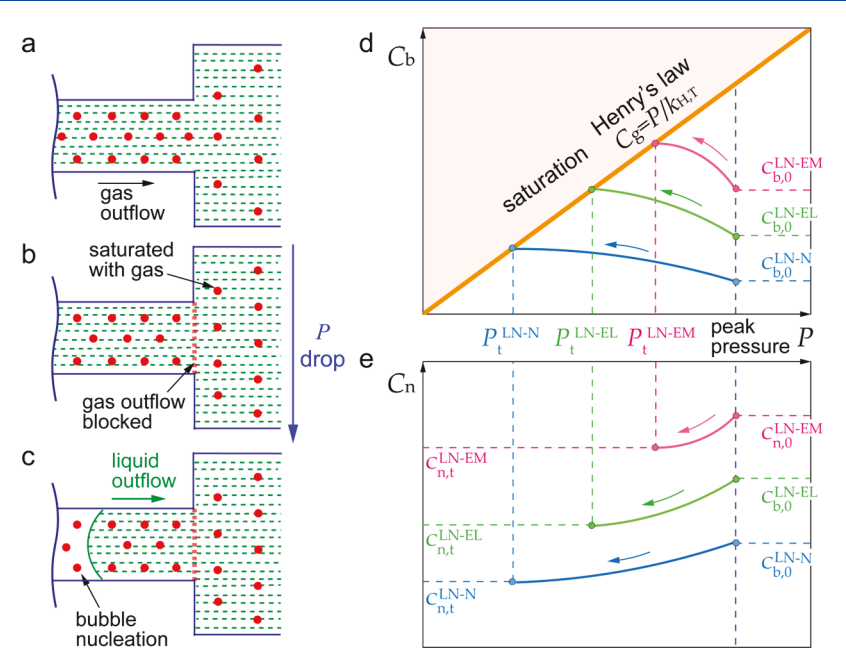


Figure 5. (a-c) Liquid outflow and bubble nucleation in nanochannels, (d) schematic of gas concentration increase contour in the bulk liquid phase, and (e) schematic of gas concentration decrease contour in the nanochannels.

and $\Delta c_{\rm n,a}$ increases with ϕ . For LN-V sample, the gas content in the LN-V has been minimized and the bulk phase will never be saturated with gas, that is $P_{\rm t}^{\rm LN-V}=0$. From eq 4 and Figure 5d, $P_{\rm t}^{\rm LN-EM}>P_{\rm t}^{\rm LN-EL}>P_{\rm t}^{\rm LN-W}>P_{\rm t}^{\rm LN-V}$. As the LN samples are completely sealed, the total gas amount is conservative. The gas amount increase in the bulk phase is equivalent to the gas amount decrease in the nanochannels. Thus, when the bulk liquid is saturated during the unloading process, the gas concentration in the nanochannels is

$$c_{n}(t_{0}) = c_{n,0} - \Delta c_{n,a} \tag{5}$$

As depicted in Figure 5e, as the gas outflow is ceased at a higher threshold pressure, more gas molecules are retained in the confined liquid, that is, $c_{\rm n,t}^{\rm LN-EM} > c_{\rm n,t}^{\rm LN-EL} > c_{\rm n,t}^{\rm LN-N} > c_{\rm n,t}^{\rm LN-V}$. At the threshold pressure, although the bulk liquid has been saturated, the gas remained in the nanochannels are still dissolved by the confined liquid because of the oversolubility in the nanoenvironment. Please note that the gas oversolubility factor in the nanochannels is of key importance to the following bubble nucleation, as more gas molecules are preserved in the nanochannels during the unloading process. ¹² In short, both $P_{\rm t}$ and $c_{\rm n}(t_0)$ increase with ϕ .

Once the gas outflow is ceased, the free energy of the confined liquid in the nanochannels starts to increase with system pressure reduction. To maintain the minimum system free energy, liquid-gas-phase separation takes place in the nanoenvironment, that is, bubble nucleation occurs (Figure 5c). According to the classic bubble nucleation theory in the absence of gas phase, 35-37 the formation of a vapor nucleus increases the system free energy by (i) $\gamma_{sv}A_{sv}$, where γ_{sv} is the solid-vapor interfacial tension and A_{sv} is the solid-vapor interface area; (ii) $\gamma_{lv}A_{lv}$, where γ_{lv} is the liquid-vapor interfacial tension and Alv is the liquid-vapor interface area; and (iii) $P_{\text{out}}V$, where P_{out} is the liquid outflow pressure and Vis the volume recovery of the LN system. On the other hand, the system free energy is reduced because of the surface hydrophobicity by $\Delta \gamma A_{ls}$, where A_{ls} is the liquid-solid interface area. Thus, a thermodynamic equilibrium is expressed as

$$\gamma_{\rm sv}A_{\rm sv} + \gamma_{\rm lv}A_{\rm lv} + P_{\rm out}V = \Delta \gamma A_{\rm ls} \tag{6}$$

The above equilibrium well describes the phase separation process in the confined nanoenvironment. However, the gas phase, which has strong interaction with the confined liquid and influences the liquid outflow behavior, exists. In this case, the confined gas solution becomes supersaturated given that no gas molecules exist in the vapor bubble. Based on Henry's law, the excessive gas molecules tend to separate from the confined liquid into the vapor phase, releasing the system free energy by $P_{\rm g}V_{\rm g}=C_{\rm n,t}k_{\rm H,T}V_{\rm g}$, where $V_{\rm g}$ is the gas volume separated from the confined liquid phase. Then, the above thermodynamic equilibrium equation is modified as

$$\gamma_{\rm sv}A_{\rm sv} + \gamma_{\rm lv}A_{\rm lv} + P_{\rm out}V = \Delta\gamma A_{\rm ls} + c_{\rm n,t}k_{\rm H,T}V_{\rm g} \tag{7}$$

from which the liquid outflow pressure is calculated as

$$P_{\text{out}} = \frac{k_{\text{H},T} V_{\text{g}}}{V} c_{\text{n,t}} + \frac{\Delta \gamma A_{\text{lv}} - \gamma_{\text{sv}} A_{\text{sv}} - \gamma_{\text{lv}} A_{\text{lv}}}{V}$$
(8)

P_{out} is promoted by the retained gas concentration in the confined liquid. This trend agrees well with our experimental results (inset in Figure 2c) as well as literature results, 40 in which the supersaturation limit pressure increases with the increase of dissolved gas concentration in bulk liquid. Thus, the bubble nucleation in the nanochannels is initiated at the pressure Pout, which has a higher value in LN sample containing higher gas content. As the system pressure reduces, the formed bubble continuously grows at the gas-liquid interface, which has the lowest energy barrier. 22,23 The bubble growth and expansion in the nanochannels is a driving force of liquid outflow, 12,25 pushing the confined liquid out of the hydrophobic nanochannels. In the bulk phase, when the system pressure reduces to a certain pressure level, the bulk liquid phase is saturated with gas. Since then, the bulk liquid phase is always saturated, forming a high energy barrier and blocking the gas outflow from the nanochannels. Following Henry's law in Figure 5d, the further reduced system pressure leads to gas precipitation and bubble formation in the bulk liquid phase.

Based on the above analysis, when the unloading starts, the gas and liquid molecules flow out from the nanochannels to the bulk liquid. The gas outflow is blocked once the bulk phase is saturated, while the liquid outflow continues. For the LN sample containing higher gas content, the gas outflow suppression (Figure 5b) as well as bubble nucleation (Figure 5c) occur at a higher threshold pressure because of the faster bulk liquid saturation and the enhanced liquid—gas interaction in the gas—supersaturated liquid in the nanochannels. Consequently, the higher system free energy reduction resulted from the release of gas molecules from confined liquid to vapor phase drives more liquid out, leading to a higher $\eta_{\rm out}$.

CONCLUSIONS

In summary, we have independently investigated the gas effect on the liquid outflow from hydrophobic nanochannels by maintaining the excessive solid—liquid interfacial tension as a constant. The degree of liquid outflow from hydrophobic nanochannels is found to be a function of the amount of gas in the LN samples. Higher amount of gas blocks the gas outflow at a higher threshold pressure and thus retains more gas molecules in the nanochannel. The additionally retained gas molecules promote the bubble nucleation process and results higher degree of liquid outflow.

ASSOCIATED CONTENT

Supporting Information

The Supporting Information is available free of charge at https://pubs.acs.org/doi/10.1021/acs.langmuir.0c00466.

Pore size distribution of the nanoporous silica used in this study and results of extra gas effect on liquid outflow behavior in another nanoporous silica-based LN system (PDF)

AUTHOR INFORMATION

Corresponding Author

Weiyi Lu — Department of Civil and Environmental Engineering, Michigan State University, East Lansing, Michigan 48824, United States; ⊚ orcid.org/0000-0003-1069-3480; Phone: (517) 353-6448; Email: wylu@egr.msu.edu

Authors

Mingzhe Li — Department of Civil and Environmental Engineering, Michigan State University, East Lansing, Michigan 48824, United States

Lijiang Xu — Department of Civil and Environmental Engineering, Michigan State University, East Lansing, Michigan 48824, United States

Complete contact information is available at: https://pubs.acs.org/10.1021/acs.langmuir.0c00466

Notes

The authors declare no competing financial interest.

ACKNOWLEDGMENTS

The authors would like to thank the financial support of National Science Foundation (NSF CBET-1803695).

REFERENCES

- (1) Heiranian, M.; Farimani, A. B.; Aluru, N. R. Water Desalination with a Single-Layer MoS 2 Nanopore. *Nat. Commun.* **2015**, *6*, 8616.
- (2) Jackson, E. A.; Hillmyer, M. A. Nanoporous Membranes Derived from Block Copolymers: From Drug Delivery to Water Filtration. *ACS Nano* **2010**, *4*, 3548–3553.
- (3) Sun, C.-Y.; Qin, C.; Wang, C.-G.; Su, Z.-M.; Wang, S.; Wang, X.-L.; Yang, G.-S.; Shao, K.-Z.; Lan, Y.-Q.; Wang, E.-B. Chiral Nanoporous Metal-Organic Frameworks with High Porosity as Materials for Drug Delivery. *Adv. Mater.* **2011**, 23, 5629–5632.
- (4) Gultepe, E.; Nagesha, D.; Sridhar, S.; Amiji, M. Nanoporous Inorganic Membranes or Coatings for Sustained Drug Delivery in Implantable Devices. *Adv. Drug Deliv. Rev.* **2010**, *62*, 305–315.
- (5) Asao, N.; Ishikawa, Y.; Hatakeyama, N.; Menggenbateer; Yamamoto, Y.; Chen, M.; Zhang, W.; Inoue, A. Nanostructured Materials as Catalysts: Nanoporous-Gold-Catalyzed Oxidation of Organosilanes with Water. *Angew. Chem., Int. Ed.* **2010**, *49*, 10093–10095.
- (6) Ding, Y.; Chen, M. Nanoporous Metals for Catalytic and Optical Applications. MRS Bull. 2009, 34, 569–576.
- (7) Vlassiouk, I.; Takmakov, P.; Smirnov, S. Sensing DNA Hybridization via Ionic Conductance through a Nanoporous Electrode. *Langmuir* **2005**, *21*, 4776–4778.
- (8) Santos, A.; Kumeria, T.; Losic, D. Nanoporous Anodic Aluminum Oxide for Chemical Sensing and Biosensors. *Trac. Trends Anal. Chem.* **2013**, *44*, 25–38.
- (9) Zhang, Y.; Li, M.; Gao, Y.; Xu, B.; Lu, W. Compressing Liquid Nanofoam Systems: Liquid Infiltration or Nanopore Deformation? *Nanoscale* **2018**, *10*, 18444–18450.
- (10) Li, M.; Li, J.; Barbat, S.; Baccouche, R.; Lu, W. Enhanced Filler-Tube Wall Interaction in Liquid Nanofoam-Filled Thin-Walled Tubes. *Compos. Struct.* **2018**, 200, 120–126.
- (11) Grosu, Y.; Mierzwa, M.; Eroshenko, V. A.; Pawlus, S.; Chorażewski, M.; Nedelec, J.-M.; Grolier, J.-P. E. Mechanical, Thermal, and Electrical Energy Storage in a Single Working Body: Electrification and Thermal Effects upon Pressure-Induced Water Intrusion-Extrusion in Nanoporous Solids. *ACS Appl. Mater. Interfaces* **2017**, *9*, 7044–7049.
- (12) Xu, L.; Li, M.; Lu, W. Effect of Electrolytes on Gas Oversolubility and Liquid Outflow from Hydrophobic Nanochannels. *Langmuir* **2019**, *35*, 14505–14510.
- (13) Li, M.; Lu, W. Liquid Marble: A Novel Liquid Nanofoam Structure for Energy Absorption. *AIP Adv.* **2017**, *7*, 055312.
- (14) Grosu, Y.; Faik, A.; Nedelec, J.-M.; Grolier, J.-P. Reversible Wetting in Nanopores for Thermal Expansivity Control: From Extreme Dilatation to Unprecedented Negative Thermal Expansion. *J. Phys. Chem. C* **2017**, *121*, 11499–11507.
- (15) Han, A.; Qiao, Y. A Volume-Memory Liquid. Appl. Phys. Lett. 2007, 91, 173123.
- (16) Han, M.; Espinosa-Marzal, R. M. Influence of Water on Structure, Dynamics, and Electrostatics of Hydrophilic and Hydrophobic Ionic Liquids in Charged and Hydrophilic Confinement between Mica Surfaces. ACS Appl. Mater. Interfaces 2019, 11, 33465—33477
- (17) Lu, W.; Kim, T.; Punyamurtula, V. K.; Han, A.; Qiao, Y. Effects of Addition of Potassium Chloride and Ethylene Glycol on Nanofluidic Behaviors. *J. Mater. Sci.* **2011**, *46*, 4053–4057.
- (18) Ryzhikov, A.; Khay, I.; Nouali, H.; Daou, T. J.; Patarin, J. Drastic Change of the Intrusion-Extrusion Behavior of Electrolyte Solutions in Pure Silica *BEA-Type Zeolite. *Phys. Chem. Chem. Phys.* **2014**, *16*, 17893–17899.
- (19) Han, A.; Lu, W.; Kim, T.; Chen, X.; Qiao, Y. Influence of Anions on Liquid Infiltration and Defiltration in a Zeolite Y. *Phys. Rev. E: Stat., Nonlinear, Soft Matter Phys.* **2008**, 78, 031408.
- (20) Rigby, S. P.; Edler, K. J. The Influence of Mercury Contact Angle, Surface Tension, and Retraction Mechanism on the Interpretation of Mercury Porosimetry Data. *J. Colloid Interface Sci.* **2002**, 250, 175–190.

- (21) Qiao, Y.; Cao, G.; Chen, X. Effects of Gas Molecules on Nanofluidic Behaviors. J. Am. Chem. Soc. 2007, 129, 2355–2359.
- (22) Lefevre, B.; Saugey, A.; Barrat, J. L.; Bocquet, L.; Charlaix, E.; Gobin, P. F.; Vigier, G. Intrusion and Extrusion of Water in Hydrophobic Mesopores. *J. Chem. Phys.* **2004**, *120*, 4927–4938.
- (23) Grosu, Y.; Ievtushenko, O.; Eroshenko, V.; Nedelec, J. M.; Grolier, J. P. E. Water Intrusion/Extrusion in Hydrophobized Mesoporous Silica Gel in a Wide Temperature Range: Capillarity, Bubble Nucleation and Line Tension Effects. *Colloids Surf., A* **2014**, 441, 549–555.
- (24) Tinti, A.; Giacomello, A.; Grosu, Y.; Casciola, C. M. Intrusion and Extrusion of Water in Hydrophobic Nanopores. *Proc. Natl. Acad. Sci. U.S.A.* **2017**, *114*, E10266–E10273.
- (25) Li, M.; Xu, L.; Lu, W. Nanopore Size Effect on Critical Infiltration Depth of Liquid Nanofoam as a Reusable Energy Absorber. J. Appl. Phys. 2019, 125, 044303.
- (26) Sun, Y.; Li, P.; Qiao, Y.; Li, Y. Time-Dependent Gas-Liquid Interaction in Molecular-Sized Nanopores. Sci. Rep. 2015, 4, 6547.
- (27) Li, M.; Lu, W. Adaptive Liquid Flow Behavior in 3D Nanopores. Phys. Chem. Chem. Phys. 2017, 19, 17167–17172.
- (28) Joseph, S.; Aluru, N. R. Why Are Carbon Nanotubes Fast Transporters of Water? *Nano Lett.* **2008**, *8*, 452–458.
- (29) Battino, R.; Rettich, T. R.; Tominaga, T. The Solubility of Nitrogen and Air in Liquids. *J. Phys. Chem. Ref. Data* **1984**, *13*, 563–600.
- (30) Hu, Y.; Huang, L.; Zhao, S.; Liu, H.; Gubbins, K. E. Effect of Confinement in Nano-Porous Materials on the Solubility of a Supercritical Gas. *Mol. Phys.* **2016**, *114*, 3294–3306.
- (31) Ho, L. N.; Schuurman, Y.; Farrusseng, D.; Coasne, B. Solubility of Gases in Water Confined in Nanoporous Materials: ZSM-5, MCM-41, and MIL-100. *J. Phys. Chem. C* **2015**, *119*, 21547–21554.
- (32) Miachon, S.; Syakaev, V. V.; Rakhmatullin, A.; Pera-Titus, M.; Caldarelli, S.; Dalmon, J.-A. Higher Gas Solubility in Nanoliquids? *ChemPhysChem* **2008**, *9*, 78–82.
- (33) Luzar, A.; Bratko, D. Gas Solubility in Hydrophobic Confinement. *J. Phys. Chem. B* **2005**, 109, 22545–22552.
- (34) Jaynes, D. B.; Rogowski, A. S. Applicability of Fick's Law to Gas Diffusion. *Soil Sci. Soc. Am. J.* **1983**, 47, 425–430.
- (35) Giacomello, A.; Chinappi, M.; Meloni, S.; Casciola, C. M. Geometry as a Catalyst: How Vapor Cavities Nucleate from Defects. *Langmuir* **2013**, *29*, 14873–14884.
- (36) Giacomello, A.; Chinappi, M.; Meloni, S.; Casciola, C. M. Metastable Wetting on Superhydrophobic Surfaces: Continuum and Atomistic Views of the Cassie-Baxter-Wenzel Transition. *Phys. Rev. Lett.* **2012**, *109*, 226102.
- (37) Han, A.; Kong, X.; Qiao, Y. Pressure Induced Liquid Infiltration in Nanopores. *J. Appl. Phys.* **2006**, *100*, 014308.
- (38) Enríquez, O. R.; Hummelink, C.; Bruggert, G.-W.; Lohse, D.; Prosperetti, A.; Van Der Meer, D.; Sun, C. Growing Bubbles in a Slightly Supersaturated Liquid Solution. *Rev. Sci. Instrum.* **2013**, *84*, 065111.
- (39) Hemmingsen, E. A. Cavitation in Gas-Supersaturated Solutions. *J. Appl. Phys.* **1975**, *46*, 213–218.
- (40) Mori, Y.; Hijikata, K.; Nagatani, T. Effect of Dissolved Gas on Bubble Nucleation. *Int. J. Heat Mass Transfer* **1976**, *19*, 1153–1159.